Experimental and numerical analysis of an air-cooled double-lift NH3-H2O absorption refrigeration system

Marcello Aprile ([1]), Tommaso Toppi, Marco Guerra, Mario Motta

Department of Energy, Politecnico di Milano, 20156 Milano, Italy

Abstract

The prototype of an air-cooled double-lift NH3-H2O absorption chiller driven by hot water at low temperature is presented. The main objective of the study is to illustrate the experimental performances of the prototype under different operating conditions. A mathematical model of the cycle is developed, along with a procedure for the identification of otherwise difficult to measure

[1] Corresponding author. Tel.: +39 02 2399 3865; fax: +39 02 2399 3868.

E-mail address: marcello.aprile@polimi.it (M. Aprile).

data, with the purpose of providing the complete picture of the internal thermodynamic cycle. The combined experimental and numerical data allowed assessing the effects on the thermodynamic cycle with varying operating conditions. The unit operated steadily with chilled water inlet 12°C, outlet 7°C, air temperature between 22°C and 38°C, and hot water driving temperatures between 80°C and 90°C. The reference cooling capacity at air temperature of 30°C is 2.5 kW, with thermal COP about 0.3 and electrical COP about 10.

1. Introduction

In the next decades, the increasing energy demand along with environmental protection measures will impose higher efficiency requirements and eco-compatibility constraints on air conditioning and refrigeration devices. Absorption cooling, combined with waste or solar heat, can become an environmentally friendly alternative to vapor compression cooling. Possible applications of the concept in the micro scale include micro-trigeneration, distributed cooling powered by district heating and solar thermal cooling.

Although promising developments have been achieved in the recent years, especially in combination with solar thermal energy (Henning et al., 2013), more research is needed in order to improve performance and lower costs of small-size applications. The key features that could improve market viability are: 1) a low driving temperature, approximately below 90°C, so to allow the exploitation of low-grade heat; 2) a compact integrated dry heat rejection device, so as to lower costs and easily comply with regulatory constraints (e.g. control of Legionella proliferation); 3) a high overall electrical COP.

Air-cooled heat rejection along with low driving heat temperature is a challenging goal for commercially available absorption cooling systems. In single effect water-LiBr chillers, crystallization is the main obstacle (Wang et al., 2011). Different techniques have been proposed in order to limit the risk of crystallization, including crystallization inhibitors, increased heat and mass transfer at the absorber, control of evaporator and generator temperature, boosting of absorber

pressure through mechanical compression. In single effect ammonia-water chillers, air-cooled heat rejection implies the raise of condenser and absorber temperatures, which in turn creates the need for high driving heat temperature well above 100°C. For both commercially available pairs, it is necessary to look for different thermodynamic cycles that show a larger thermal lift. Double-lift cycles are suited for the goal. They can be defined as two-stage cycles that perform condensation or absorption at temperature level below that of the ambient through an internal heat exchange. Alefeld and Radermacher (1993) have described the three conventional double-lift cycles. The thermal COP can be assessed with the superposition method, as explained by Ziegler and Alefeld (1987). Fig. 1 shows the schematic representation in the ammonia-water P-T-X diagram of the three conventional double-lift cycles operating at the same three temperature levels (0°C, 50°C and 80°C). Each cycle is represented as the superposition of two elementary cycles. Solid arrows indicate the heat loads of the first cycle (the one providing useful cooling effect), dashed arrows those of the second cycle, and dotted arrows the internal heat exchange. Cycle A (pressure-staged) can be seen as the cascade of two single-effect refrigeration cycles, A1 and A2, where the evaporator of A2 is thermally coupled to the absorber of A1. The overall thermal COP can be estimated like $COP_{t,R}/(1 + 1/COP_{t,R})$. In cycle B (vapor-exchange), B2 evaporator is thermally coupled to B1 condenser. In this case, the overall thermal COP is $COP_{t,R}/2$. Finally, cycle C (resorption) can be seen as the superposition of a refrigeration cycle (C1) and a heat transformer cycle (C2), in which C1 condenser provides the heat input to C2 and the heat rejected at C2 condenser diminishes the cooling effect of C1. The overall thermal COP is $COP_{t,R}COP_{t,T}$.

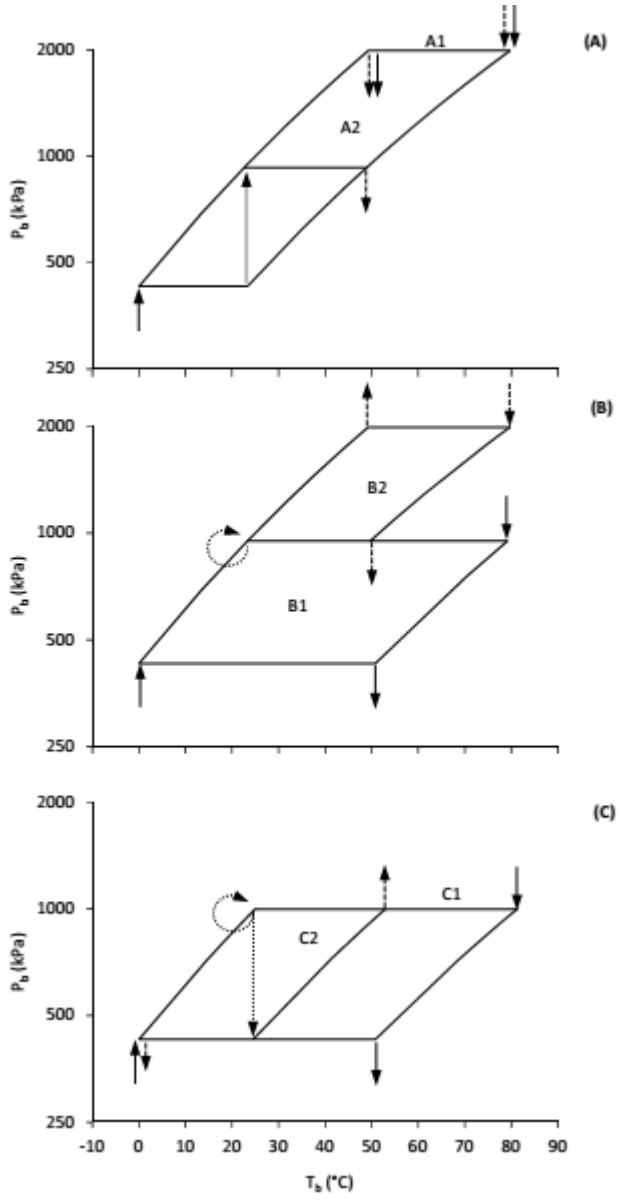

Fig. 1 – Conventional double-lift cycles

According to this simplified analysis, cycle B promises to reach the highest thermal COP. However, other factors shall be taken into consideration when comparing different cycles, e.g. rectification and circulation losses, minimum generation temperature, heat duty, cycle stability, electrical COP. In the past, the real implementations of these cycles have been investigated both theoretically and experimentally. Erickson and Tang (1996) theoretically evaluated different variations of the conventional double-lift cycles working with the ammonia-water pair, including three different solution paths of the pressure-staged cycle (parallel flow, single pump series flow, two pump series

flow), an improved vapor-exchange cycle, a resorption cycle and the so called semi-GAX cycles. The authors concluded that the semi-GAX cycle (a variant of the vapor-exchange cycle that incorporates the GAX concept) was the most efficient, although the pressure-staged two pump series flow had the advantage of the lowest generation temperature.

Kim and Infante Ferreira (2005) experimentally investigated a water-LiBr half-effect cycle of the pressure-staged type with parallel solution flow and active control of the distribution between intermediate pressure and low pressure refrigerant lines. The authors reported a thermal COP of 0.25 for a prototype unit of 4.4 kW.

Du et al. (2012) have carried out experimental studies on an ammonia-water vapor-exchange prototype unit of 2 kW cooling capacity. The authors reported a thermal COP of 0.21 and an electrical COP of 5.1 with feeding hot water of 85 °C, air temperature of 29 °C and evaporating temperature of 8 °C.

In the field of pressure-staged dual-lift water-ammonia cycles, an improved concept of low temperature driven air-cooled absorption chiller has been recently proposed (Guerra, 2012a) and first experimental activities have been performed (Guerra, 2012b). This cycle is similar in principle to the two-pump series-flow cycle, with a major difference: the refrigerant leaving the condenser is not split through a valve but is entirely routed to the low-pressure absorber where only a fraction evaporates. Doing so, the remaining liquid can be easily separated by the vapor through a phase separator, with the advantage of a self-adjusting refrigerant split that enhances both performance and cycle stability.

In the present work, an experimental and numerical analysis on this novel concept is carried out. On the one hand, the experimental work allows the performance assessment of the absorption chiller under different operating conditions by measuring cooling capacity, heat input, power consumption, internal temperatures and pressures. On the other hand, the numerical analysis allows the evaluation of otherwise difficult to measure mass flow rates and concentrations in the main cycle state points by means of an identification procedure based on the available experimental data. Finally, the study

illustrates how the performance of the absorption chiller is influenced by different operating strategies with the aim of optimizing the chiller electrical COP.

2. Experimental apparatus

In this section, the features of the chiller prototype are presented, along with the thermodynamic cycle. Moreover, the test apparatus and its measurement accuracy are briefly described. Finally, the test activities are introduced.

2.1. Chiller prototype

A simplified scheme of the prototype implementing the new cycle is given in Fig. 2. The distinguishing feature of the cycle consists in routing the entire flow rate of the liquid refrigerant leaving the condenser (CON) to cool, at an intermediate pressure, the solution in which the low pressure refrigerant vapor is absorbed after leaving the evaporator (EVA). Such operation takes place inside a tube-in-tube counter-flow refrigerant cooled absorber (RCA), in which the amount of liquid refrigerant evaporated at the intermediate pressure depends, at a given operating condition, on the amount of low pressure vapor to be absorbed. The evaporated refrigerant, separated from the liquid fraction (SEP), is absorbed in the air cooled absorber (ABS) whereas the liquid fraction is expanded to low pressure (RS2), reaching the evaporator inlet (EVA). The weak solution leaving the generator is partially enriched in the refrigerant cooled absorber, pumped to intermediate pressure (P1) and routed to internal heat recovery (SHE1) and rectifier (REC). The solution is finally enriched in the air cooled absorber, pumped (P2) to high pressure and routed to the generator (GEN) passing through a second internal heat recovery stage (SHE2). Fig. 3 qualitatively represents the thermodynamic cycle in the P-T-X diagram. One interesting characteristic of this cycle is the interdependence between refrigerant stream and solution stream in the RCA. At parity of other conditions, the intermediate pressure drives the evaporation of refrigerant in the RCA. The fraction of liquid refrigerant remaining at RCA outlet evaporates in the EVA and is eventually

absorbed in the solution stream through the RCA. Therefore, it can be said that the intermediate pressure self-adjusts so that the amount of refrigerant evaporated at intermediate pressure counterbalances the amount of refrigerant absorbed at low pressure.

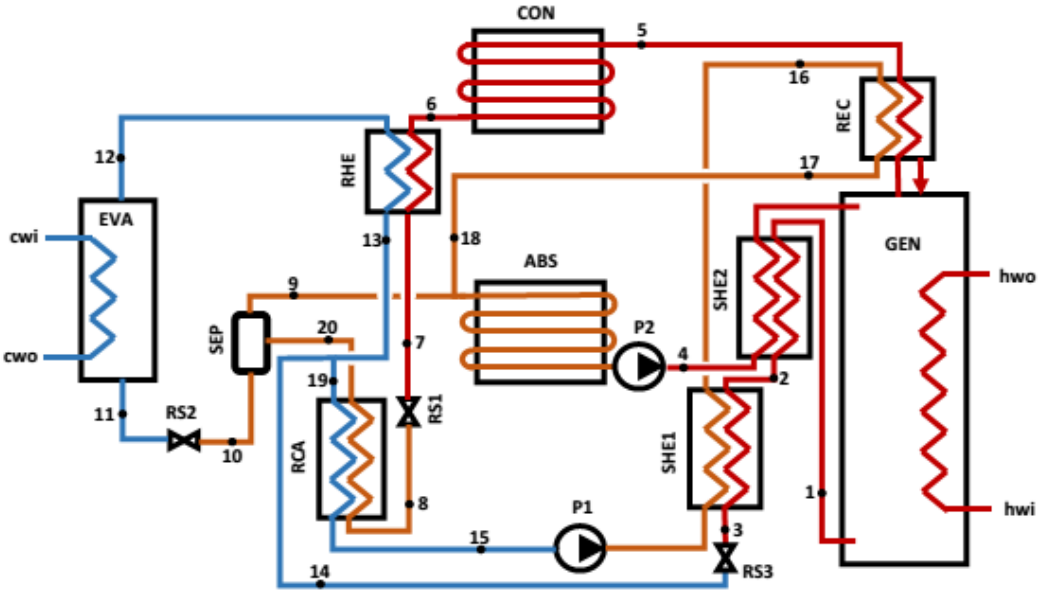

Fig. 2 – Scheme of the chiller prototype

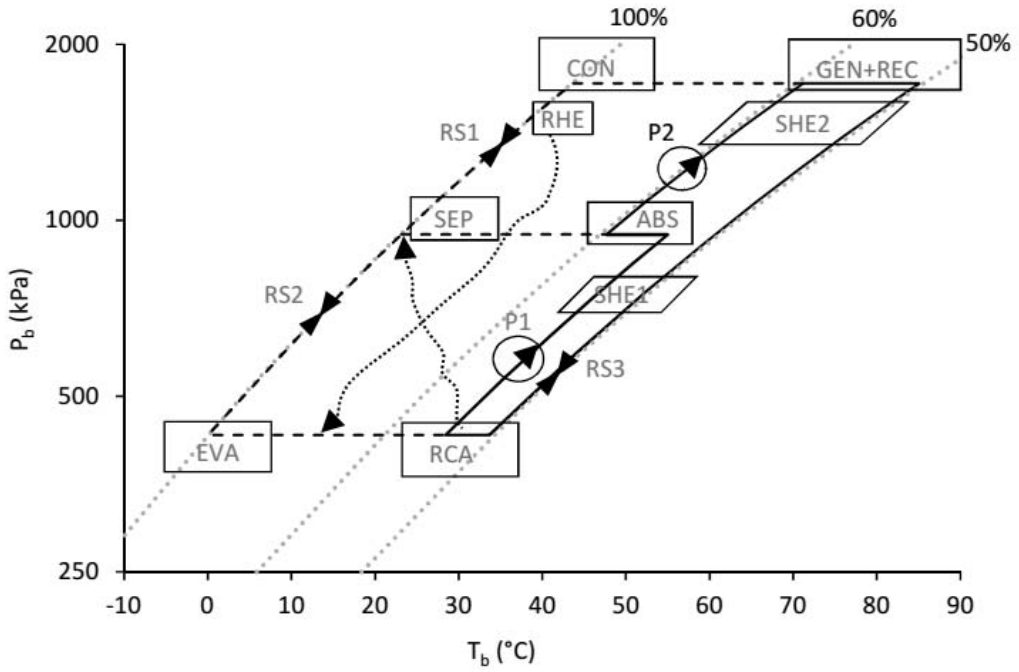

Fig. 3 – P-T-X diagram of the cycle

A small scale prototype of the cycle has been constructed (Guerra, 2012b) and its main features are hereafter described. The generator is a vertical shell-and-tube falling-film heat exchanger. The liquid rich solution flows down from the liquid distributor along the internal side of the vertical tubes, heated by hot water circulating counter flow on the external side of the tubes. The weak solution is collected at the bottom, whereas desorbed vapor flows upwards and is collected at the top. Heat exchangers SHE1, SHE2 and RCA are tube-in-tube, horizontal flow. The evaporator is a shell-and-tube vertical flow countercurrent heat exchanger, in which refrigerant liquid and vapor flow in co-current mode. Condenser and absorber are steel tubes coils with vertical aluminum fins. Tubes are horizontal and arranged in one row, cooled by a 500 mm axial fan. The rectifier is made of a pall ring packed bed with solution cooled coil. Restrictors RS1, RS2 and RS3 are made of series of drilled disks. Finally, P1 and P2 are membrane pumps, hydraulic oil driven, with a single inverter controlled motor (100 W max. power). In the present work, solution charge, pumps speed and restrictors have been set in order to optimize the electrical COP at the selected reference conditions.

2.2 Measurement apparatus

The chiller prototype was equipped with thermocouples (T type, accuracy 0.4°C) in correspondence to the state points as shown in Fig. 2. Moreover, capacitive pressures probes (accuracy 0.25% of pressure span) have been used to measure condenser pressure (position 5, ±6 kPa), separator pressure (position 9, ±4 kPa), evaporator pressure (position 12, ±2.5 kPa), absorber outlet pressure (inlet of pump P2, ±4 kPa) and RCA solution outlet pressure (position 15, ±2.5 kPa).

Temperatures and flow rates of the external water circuits are measured by thermoresistances (PT100, accuracy 0.1°C) and magnetic flowmeters (accuracy 2.5%), respectively. Overall uncertainty on heat transfer rates measurements is about 3.5%. The unit was tested in a climatic chamber (see Fig. 4) which is capable of controlling air temperature in a very stable way, with temperature deviations within ±0.1 K throughout the test period.

2.3 Test plan

The main purpose of the experimental tests is to characterize the steady-state chiller performance in terms of cooling capacity, thermal COP and electrical COP with varying air temperature, hot water temperature at generator inlet, hot water temperature drop between generator inlet and outlet, and fan speed. Thermal COP is calculated as the cooling capacity to heat input ratio, whereas electrical COP is here defined as the cooling capacity to power input ratio. Power input includes electricity consumption for the fan and the two solution pumps.

Preliminary tests are carried out in order to adjust the solution charge, after which the charge is no longer modified. During all other tests, chilled water inlet and outlet temperatures are maintained fixed at 12°C and 7°C, respectively.

The first objective is the characterization of the unit at the reference operating conditions. In this test, hot water inlet temperature is set at 90°C with a temperature drop of 10°C through the generator (low flow test). For simplicity, pumps and fan are operated at constant speed.

In a second phase, the effect of the fan speed on the chiller performance is investigated. External temperatures are kept constant while the fan speed is varied. The goal is to measure the variation of electrical COP and cooling capacity with varying the fan air flow and the associated auxiliary energy consumption.

Finally, the performance with varying hot water inlet temperature and temperature drop at the generator is assessed. In particular, temperature drop is varied from 10°C to 5°C (high flow test) and different inlet temperatures (80°C and 85°C) are tested.

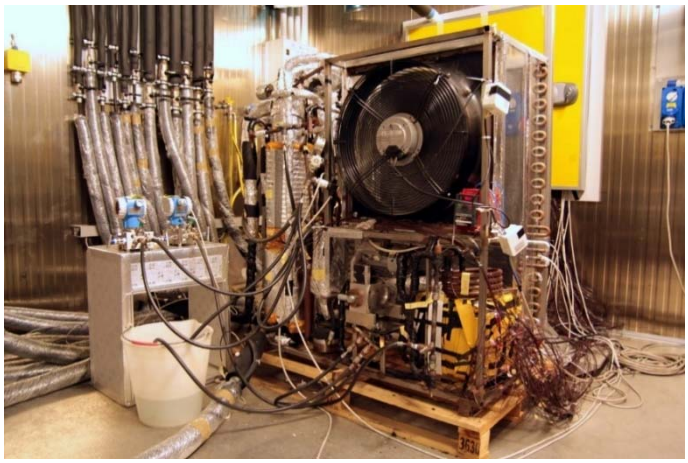

Fig. 4 – Prototype under test

3. Mathematical model

A mathematical model of the cycle is developed and implemented in FORTRAN code. The modelling approach is described hereafter, along with the technique used for the model calibration against the experimental data.

3.1 Modelling approach

The cycle state points are calculated by simultaneously solving a set of nonlinear algebraic equations, which derive in principle from steady-state balance of mass, species, enthalpy and momentum across each component. The independent variables are enthalpy (h), pressure (P), mass fraction (X) and mass flow rate ($\dot{m}$) in each cycle point. The assumptions under which the equations are derived are:

1) steady state is achieved;
2) liquid and gas phases that coexist in a cycle state point are in phase equilibrium;
3) kinetic energy and potential energy have a negligible influence;
4) pressure drops in the connecting pipes are negligible;
5) thermodynamic equilibrium properties follow the correlations in (Ziegler and Trepp, 1984).

Following the modular approach used by the ABSIM simulation tool (Grossman and Zaltash, 2001), the set of equations is derived in a systematic manner. For each component, inlet and outlet ports are identified according to the direction of mass flow rate. The integral mass, species and energy conservation equations are imposed in order to calculate the independent variables $\dot{m}$, X and h at each component outlet (forward propagation). Additional equations are needed according to the specific function of each component, e.g. heat transfer rate for heat exchangers, work input for pumps, equilibrium conditions for phase separators. Regarding the calculation of pressures, a relationship between pressure drop and flow is not considered in most components. On the one hand, pressures drop are in many cases negligible (zero or very small values); on the other hand, pressure drops are in some cases (i.e. where the solution flashes) difficult to predict. Therefore, alternative conditions (e.g. degrees of refrigerant subcooling at the inlet, fixed pressure at the outlet) are set in order to replace the missing pressure drop equations.

3.1.1 Generic component model

Within a component, there might be one or more non-mixing solution streams. Typically, internal heat exchangers have two non-mixing solution streams whereas external heat exchangers have only one solution stream. The general form of the integral mass, species and energy conservation equations applying to each solution stream are:

$$\sum_{i=1}^{Ns} \dot{m}_i = 0 \qquad (1)$$

$$\sum_{i=1}^{Ns} \dot{m}_i X_i = 0 \qquad (2)$$

$$\sum_{i=1}^{Ns} \dot{m}_i h_i + Q + W = 0 \qquad (3)$$

Additionally, a pressure drop condition is imposed between inlet(s) and outlet(s) of each stream.

The generic component model is adapted to each cycle component as follows.

3.1.2 Heat exchangers

The heat transfer rate (Q) is calculated from simple $\varepsilon - NTU$ relationships (Incropera et al., 2007), in which the heat capacity rate is approximated like $\dot{m}\,|h_o - h_i| \,/\, |T_o - T_i|$ and the overall heat transfer coefficient (UA) is an unknown model parameter. Depending on the heat capacity ratio (C_r), either the $\varepsilon - NTU$ expression for the case of one fluid in phase transition (C_r=0) or that valid for single phase streams (C_r>0) is used. It shall be noticed that the purpose of the model is to identify heat transfer rates rather than UA values. Therefore, the simplified $\varepsilon - NTU$ approach is only a convenient way of calculating suitable heat transfer rates during the iterative solution of the system of equations. The heat transfer rate in the evaporator (EVA) is derived by imposing pressure (known by measurements) and outlet temperature (supposed equal to chilled water inlet temperature). This simple model assumes that, while a certain temperature difference between chilled water outlet and refrigerant inlet drives the heat-transfer duty of the evaporator, outlet vapor quality is limited by chilled water inlet temperature due to the temperature glide of the refrigerant, which can be large even at ammonia mass fractions above 99.5%. In such condition, setting an equal temperature for refrigerant outlet and chilled water inlet does not introduce appreciable errors. Of course, in certain critical situations (e.g., evaporator flooding) this simplifying assumption would provide unrealistic results. Concerning pressure drop conditions, fixed pressure drops (also known by measurements) are assigned to the solution streams of RCA and ABS, whilst the pressure drops occurring across all other heat exchangers paths are neglected.

3.1.3 Falling film generator

The scheme of the falling film generator is shown in Fig. 5. Pressure is assumed uniform all over (P_{GEN}). The strong solution at inlet (state 1) can be subcooled or in boiling state. In the latter case, phase separation is assumed at the inlet. The liquid phase (state 1L) mixes adiabatically with the liquid solution returning from the rectifier (state 2), giving rise to state 5.

$$\dot{m}_{1L} = (1 - x_1)\,\dot{m}_1 \quad (4)$$

$$X_5 = (\dot{m}_{1L}X_{1L} + \dot{m}_2X_2)/(\dot{m}_{1L} + \dot{m}_2) \quad (5)$$

$$h_5 = (\dot{m}_{1L}h_{1L} + \dot{m}_2h_2)/(\dot{m}_{1L} + \dot{m}_2) \quad (6)$$

The resulting mixture flows downwards, countercurrent to the heating water stream, heats up and reaches boiling point (5B). Vapor evolves and flows upwards (state 7), where it mixes with vapor in state 1G, giving rise to state 4.

$$\dot{m}_{1G} = x_1\,\dot{m}_1 \quad (7)$$

$$X_4 = (\dot{m}_{1G}X_{1G} + \dot{m}_7X_7)/(\dot{m}_{1G} + \dot{m}_7) \quad (8)$$

$$h_4 = (\dot{m}_{1L}h_{1G} + \dot{m}_7h_7)/(\dot{m}_{1G} + \dot{m}_7) \quad (9)$$

Weak solution is collected at the bottom and exits in state 3. In principle, a heat transfer relationship is needed to determine state 3, i.e. $Q_{GEN} = UA\,\Delta T_{lm}$, where the log mean temperature difference is based on T_{hwi}, T_{hwo}, and solution temperatures at point 5 and 3. However, it is more practical to directly assign the equilibrium temperature in state 3 as an input for the model and calculate the heat input at the generator as follows.

The mass fraction and enthalpy of state 3 can be calculated by equilibrium condition:

$$X_3 = X_L(P_{GEN}, T_3) \quad (10)$$

$$h_3 = h_L(P_{GEN}, T_3, X_3) \quad (11)$$

State 7 is derived assuming temperature equilibrium between vapor in state 7 and solution boiling point (5B) and calculating vapor mass fraction as the average of equilibrium vapor mass fractions at the beginning (5B) and the end (3) of the desorption process, i.e.:

$$T_7 = T_{5B} \quad (12)$$

$$X_7 = 1/2(X_{5BG} + X_{3G}) \quad (13)$$

Mass flow rates in state 3 and state 7 can be derived from mass and species balance equations:

$$\dot{m}_3 + \dot{m}_7 = \dot{m}_5 \quad (14)$$

$$\dot{m}_3X_3 + \dot{m}_7X_7 = \dot{m}_5X_5 \quad (15)$$

Finally, energy balance provides the heat input at the generator:

$$Q_{GEN} = \dot{m}_3 h_3 + \dot{m}_7 h_7 - \dot{m}_5 h_5 \qquad (16)$$

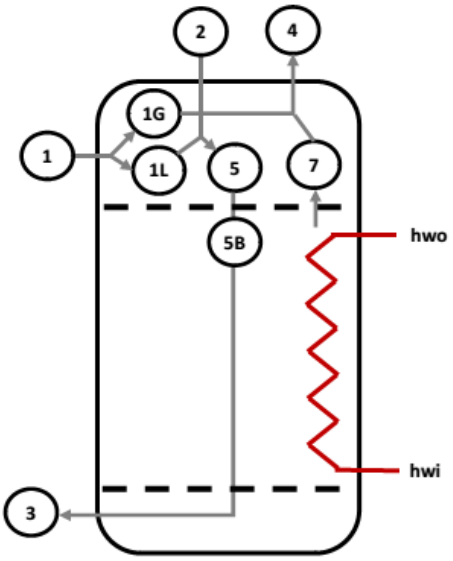

Fig. 5 – Scheme of the falling film generator

3.1.4 Separator

In the separator, pressure and temperature are assumed uniform and equilibrium conditions apply for the determination of liquid and gas mass fractions. Enthalpy in each phase is easily derived and vapor quality is calculated as:

$$x = \frac{h - h_L}{h_G - h_L} \qquad (17)$$

Finally, enthalpy, mass fraction, pressure and mass flow rates are imposed at the liquid and gas outlets.

3.1.5 Rectifier

The rectifier is treated like an internal heat exchanger with fixed UA value, followed by a phase separator. Gas phase is routed to the condenser, liquid phase returns to the generator.

3.1.6 Pumps

The balance equations (1), (2) and (3) apply also to pumps, setting heat input to zero and calculating mechanical power input like:

$$W = \frac{1}{\eta}\dot{m}/\rho(P_o - P_i) \qquad (18)$$

where η is the pump efficiency.

Concerning the determination of flow rates, a relationship on flow rate should be introduced for the pumps P1 and P2. However, it should be noticed that pumps have a limited capacity to determine the flow rates in absorption cycles. In particular, P1 and P2 interact with each other, and their volumetric capacity provides a maximum limit rather than the actual value of volume flow rates. Since convergence problems may arise if incorrect flow rates are simultaneously imposed at the two pumps, it is convenient to opt for a set of alternative conditions, i.e.:

1) degree of subcooling of the solution at pump P1 inlet;

2) volume flow rate of pump P2.

3.1.7 Restrictors

The balance equations (1), (2) and (3) apply also to restrictors, for which work and heat inputs are set to zero. Additionally, a relationship between pressure drop and flow should be introduced. Concerning restrictor RS3, the solution at the outlet should be in liquid state. In such condition, assuming fluid incompressibility, negligible effect of fluid thermal expansion, and constancy of the discharge factor through the restrictor at high Re numbers (>10^5), a simple relationship can be used:

$$\dot{m} = k\sqrt{\rho(P_i - P_o)} \qquad (19)$$

where k is a dimensional coefficient (m^2) that characterizes the restrictor.

For the other two restrictors in the cycle, RS1 and RS2, refrigerant flashes at the outlet. In this case, it is not easy to derive a simple and accurate model of the pressure drop relationship due the complex interaction among the different series connected disks comprising the restrictors (Kojasoy

at al., 1997). To overcome this problem, specific alternative conditions have been set instead of the pressure drop relationships, namely:

1) subcooling at the inlet of restrictor RS1;
2) pressure at the outlet of restrictor RS2.

3.2 Equation counting

The modular approach of equation writing would provide redundant mass balance and species balance equations. In the general case, the number of redundant equations is a multiple of two, depending on the specific cycle configuration, as pointed out in (Herold et al., 1996). For the cycle being studied there are two redundant equations, which have been identified in the mass balance and species balance at the connection node between ABS outlet and P2 inlet.

3.3 Calibration of the mathematical model

The main purpose of the numerical model is to estimate the mass flow rates and mass fractions in the cycle state points. For each test condition, the available measured data are heat input at the generator (Q_{GEN}), cooling capacity (Q_{EVA}), temperatures and flow rates of external water circuits, air temperature in the test chamber, internal temperatures and pressures in the relevant cycle points. The thermodynamic cycle state points can be identified by finding the solution vector of the main model parameters ($\tilde{\mathbf{z}}$) that minimizes the quadratic error between model predicted data (i.e., Q_j, P_k, T_l) and experimental data (i.e., $\hat{Q}_j, \hat{P}_k, \hat{T}_l$):

$$\mathrm{F}(\mathbf{z}) = \sum_{j=1}^{N_Q} w_{Qj}\left(Q_j - \hat{Q}_j\right)^2 + \sum_{k=1}^{N_P} w_{Pk}\left(P_k - \hat{P}_k\right)^2 + \sum_{l=1}^{N_T} w_{Tl}\left(T_l - \hat{T}_l\right)^2 \qquad (20)$$

where w_{Qj}, w_{Pk} and w_{Tj} are proper normalization weights. The vector of the main model parameters ($\mathbf{z}$) consists of:

1) UA value of condenser;

2) UA value of absorber;

3) UA value of RCA;

4) UA value of rectifier;

5) UA value of SHE1;

6) UA value of SHE2;

7) temperature of solution at generator outlet;

8) subcooling of solution at RCA outlet;

9) volume flow rate of strong solution ($\dot{V}_4$).

The remaining model parameters, i.e. evaporator pressure, subcooling at RS1 inlet and UA-value of RHE, were not allowed to vary during the optimization. Evaporator pressure and subcooling at RS1 inlet have been set based on the experimental data, while an average constant value for the UA of RHE was estimated, as the model turned out to be not very sensitive to this parameter.

It is noticed that the available experimental data would not allow determining the flow rates in each branch of the cycle in a straightforward manner, as explained further below.

Concerning the refrigerant side of the cycle, an indirect measure of refrigerant flow rate in the evaporator can be obtained from the cooling power, separator pressure and evaporator pressure. In fact, the refrigerant leaving the separator can be assumed in saturated liquid state with mass fraction close to unity (greater than 99%). Moreover, in the normal operation, the refrigerant leaving the evaporator is a two-phase mixture with a very large vapor quality (95% or more), and temperature very close to the chilled water inlet temperature. Therefore, the refrigerant enthalpy can be derived with very good accuracy at evaporator inlet and outlet thanks to the knowledge of separator and evaporator pressures, providing the necessary data for the mass flow rate calculation. For example, assuming uncertainty of 1% on pressures, 3% on cooling capacity and 2% on mass fractions, the overall uncertainty on refrigerant flow rate through the evaporator would be about 5%. However, the refrigerant flow rate through the condenser cannot be easily assessed with the available experimental data, because the experimental value of the heat transfer rate at the condenser is not

available. Moreover, estimating mass flow rates in the solution side of the cycle (strong, intermediate and weak) is even more complicated. In order to calculate the solution flow rates, the corresponding mass fractions should also be determined. Although the mass fraction of the weak solution can be estimated based on generator pressure and solution temperature at generator outlet, the mass fractions of intermediate and strong solutions, and consequently the respective mass flow rates, depend on the degrees of subcooling at absorber and RCA outlets, which are unknown.

In order to overcome the indetermination of the solution flow rates, it is assumed that the mass flow rate of the weak solution in RS3 follows Eq. (19) and the value of the coefficient k is the same for all tests. The determination of a proper value for the coefficient k can be achieved by the following arguments. At parity of other conditions, solution flow rates are directly proportional to the value of the coefficient k. A very large value of k would result in a volume flow rate higher than the maximum the pump P2 can provide. The limitation on the pump flow rate is imposed by the speed of the pump's drive. On the contrary, a very low value of k would decrease the solution flow rates, shifting the strong solution mass fraction towards high values. In this case, the limitation is imposed by the initial charge of the solution. Therefore, the choice of k is reflected in the ability of the numerical model to fit the experimental values.

The effects of the choice of the coefficient k are shown in Fig. 6, in which the root mean square error related to a sample test condition ($RMSE_i$) is calculated as:

$$RMSE_i = \sqrt{\frac{1}{(N_Q + N_P + N_T)} F_i(\tilde{\mathbf{z}}_i)} \qquad (21)$$

The weights in the expression for $F_i(\boldsymbol{z})$, see Eq. (20), are chosen so that a RMSE of one is equivalent to a root mean square deviation of 1 K for temperatures. Therefore, the weights for temperatures (w_{Tl}) were set to 1 K^{-2} and the remaining weights have been assigned according to the following identity based on the accuracy of the individual measurements (a_T, a_{Pk}, a_{Qj}):

$$w_{Pk} a_{Pk}^2 = w_{Qj} a_{Qj}^2 = a_T^2 \qquad (22)$$

It is observed that the value of RMSE initially decreases with k, up to the point where the volume flow rate of the pump P2 reaches the maximum value, set to 125 l/h. Consequently, RMSE departs from the minimum value (see Fig. 6).

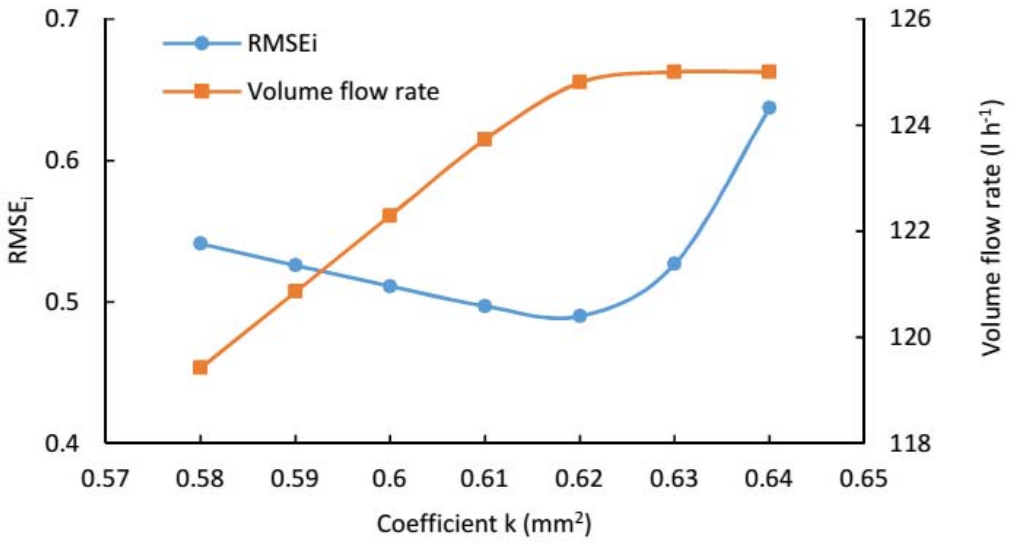

Fig. 6 – Effect of the coefficient k

Based on these arguments, an iterative identification procedure was defined:

1) Representative steady state tests are selected.
2) A tentative value is assigned to the coefficient k of restrictor RS3.
3) For each test belonging to the representative set of N_s steady state tests, the identification of the model parameters $(\tilde{\mathbf{z}}_i, i = 1 \cdots N_s)$ is performed. During the identification, a constraint on the known maximum volume flow rate of pump P2 is set:

$$\dot{V}_4 \leq 125\ (l\ h^{-1}) \qquad (23)$$

4) The average RMSE of the representative tests is calculated:

$$\overline{RMSE} = 1/N_s \sum_{i=1}^{N_s} RMSE_i \qquad (24)$$

5) A new value of k is assigned and steps 3 and 4 are repeated.

6) The most probable value of k is the one providing the minimum average RMSE.

The results of the identification procedure is shown in Fig. 7. The figure suggests that a proper value of k is about 0.60 – 0.63 mm^2. Table 1 reports the comparison between relevant experimental and numerical data for the representative set of steady state tests. The numerical data were obtained with k equal to 0.62 mm^2.

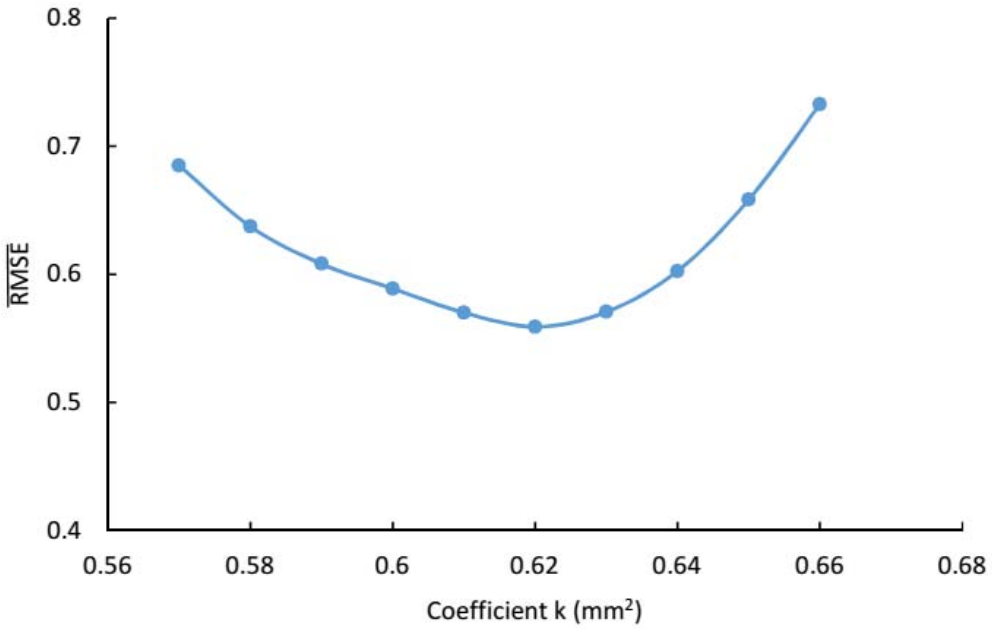

Fig. 7 – Average RMSE

Table 1 – Experimental data and model results

T_{hwi}	T_{hwo}	T_{air}	W_{aux}	Q_{EVA} (kW)		Q_{GEN} (kW)		P_{EVA} (kPa)		P_{SEP} (kPa)		P_{CON} (kPa)		RMSE
(°C)	(°C)	(°C)	(W)	exp.	mod.	exp.	mod.	exp.	mod.	exp.	mod.	exp.	mod.	-
92.3	87.3	35.1	382	2.85	2.86	9.84	9.50	514	515	1027	1040	1812	1826	0.48
80.1	70.9	22.1	158	2.32	2.32	7.51	7.37	400	400	779	793	1397	1405	0.40
79.9	70.1	27.0	225	1.94	1.95	6.67	6.49	401	400	780	794	1392	1411	0.55
79.6	70.0	30.0	349	1.60	1.60	6.00	5.80	397	398	784	804	1403	1434	0.79

80.0	70.5	31.9	350	1.26	1.27	5.36	5.18	404	405	804	793	1446	1478	0.91
84.5	75.2	31.9	359	2.15	2.15	7.44	7.21	444	445	872	892	1551	1565	0.52
85.3	80.3	35.0	368	2.02	2.02	7.49	7.15	482	482	946	973	1684	1712	0.73
85.0	79.8	38.0	416	1.43	1.43	6.25	5.92	489	489	972	1009	1734	1774	0.89
90.0	80.0	30.0	261	2.58	2.59	8.80	8.58	436	436	892	905	1617	1622	0.40

4. Results and analysis

During the tests, the unit turned out to perform smoothly and to be able to adjust quickly to changing operating conditions. The time requested to reach stability (i.e., 95% of steady state cooling capacity) after a step change of the generator temperature was, on average, less than 4 minutes. In the following, the main experimental results of the steady state tests are shown along with the P-T-X representation of the solution cycle, an outcome of the mathematical model.

4.1. Charge selection tests

The amount of ammonia charged in the system can have a strong influence on performances. It shall be noticed that the unit does not have a refrigerant buffer besides the natural buffer due to the internal volume of heat exchangers and connecting pipes. Moreover, the three restrictors have fixed geometry. With increasing amount of ammonia in the solution charge, the three pressure levels increase as well. At parity of other conditions, an increase of both the intermediate and the low pressure levels allows increasing the amount of vapor refrigerant absorbed by the two absorbers (ACA and RCA). In principle, a positive effect on cooling capacity occurs. However, at high air temperatures, the raise of the low pressure level reduces the driving temperature difference at the evaporator and, consequently, hinders the evaporation of the incoming refrigerant flow (evaporator flooding).

Compared to previous experimental works on the same chiller prototype (Guerra, 2012b), a different charge optimization is pursued in this work. A challenging test condition is selected with the aim of optimizing cooling capacity at 7°C feed water temperature and with relatively high

ambient temperatures. Air temperature is set to 38°C, with hot water inlet temperature to 90°C and chilled water inlet temperature to 12°C. Water flow rates are varied in order to reach temperature drops of 5 K at both hot water outlet and chilled water outlet. Fan power consumption is set to 340 W, close to maximum power. Ammonia charge is constantly increased until evaporator flooding is observed (see Table 2). In fact, the drop in cooling capacity from test #1 to test #2 can be explained as follows. With a higher ammonia charge, solution mass fractions are shifted to the left in the P-T-X diagram (see Fig.3), and the temperature difference between solution at RCA outlet and refrigerant at RS1 outlet diminishes. With a reduced heat transfer potential, the RCA is no longer able to absorb the refrigerant vapor leaving EVA, and evaporator pressure increases until a new equilibrium is achieved. It is noticed (see test #3) that a small increase of chilled water inlet (and outlet) temperature allows the evaporator to regain heat transfer potential and, consequently, cooling capacity. The preliminary tests suggests that, for the desired chilled water temperatures 12°C inlet, 7°C outlet, the charge in test #2 is too high and the lower charge of test #1 is restored. This choice leads to a chiller of lower cooling capacity, but with larger margin for electrical COP optimization.

Table 2 – Results of preliminary tests (experimental)

#	Q_{EVA} (kW)	COP_t (-)	COP_e (-)	Q_{GEN} (kW)	P_{EVA} (kPa)	P_{SEP} (kPa)	P_{GEN} (kPa)	T_{hwi} (°C)	T_{air} (°C)	T_{cwi} (°C)
1	2.139	0.259	4.59	8.243	491	1011	1825	90.2	38.0	12.1
2	1.603	0.177	3.77	9.065	570	1090	1833	90.1	38.0	12.1
3	2.381	0.279	5.47	8.537	543	1066	1864	90.1	38.0	13.3

4.2 Reference operating conditions

Reference operating conditions are chosen with the aim of achieving a good electrical COP with a simple control strategy. In the driving hot water loop, a large temperature drop is essential in order to reduce the parasitic energy consumption of the circulation pump. Therefore, the hot water temperature at generator inlet is set to 90°C with a temperature drop of 10°C at generator outlet.

Both fan speed and solution pumps speed are set to a moderate, constant value. The measured electricity consumption is 175 W for the fan, 85 W for the two solution pumps.

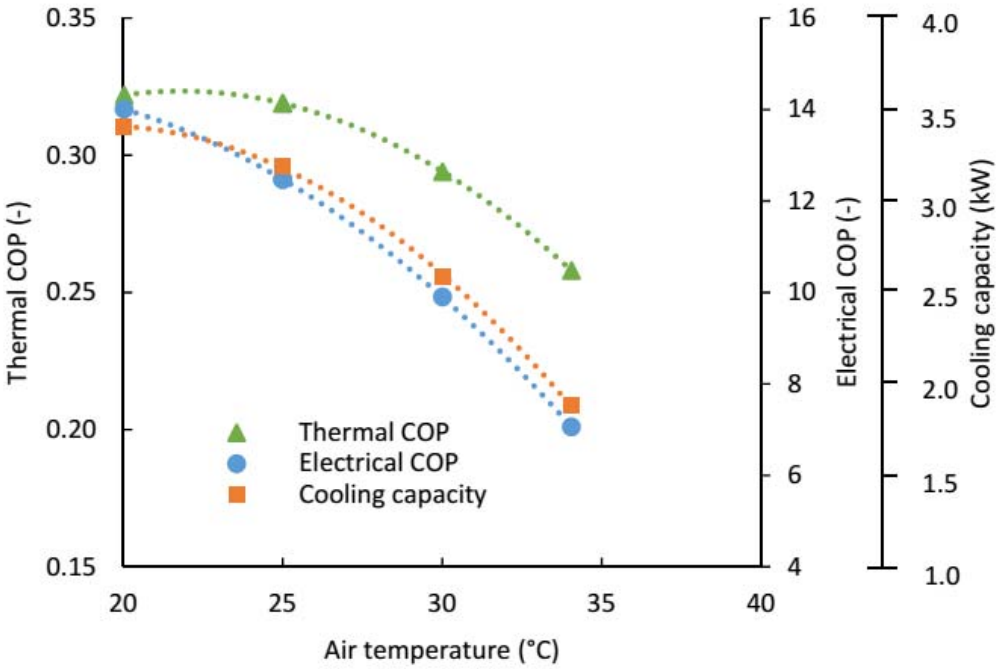

Fig. 8 – Performance at reference operating conditions (experimental)

The cooling capacity of the unit is 2.5 kW at the reference air temperature 30°C (see Fig. 8), with thermal COP of 0.29 and electrical COP of about 10. Around the reference point, cooling capacity, thermal COP and electrical COP drop sharply with air temperature. The respective percentage decrease per air temperature degree is approximately 5.8% K^{-1}, 2.3% K^{-1} and 6% K^{-1}. Performances tend to level-off for air temperatures below 27°C. The augmented absorption capacity with low ambient air temperature is responsible for the progressive decrease of evaporator pressures, as can be seen in Fig. 9. In principle, low air temperatures provide the potential for enriching the strong solution. However, due to the fixed refrigerant charge, the enrichment of the strong solution cannot be completely achieved and, as consequence, the evaporator pressure drops. As low evaporation temperatures correspond to low pressures, the overall effect is the increase of the temperature difference between refrigerant and the chilled water. In such conditions, the exergetic potential of

cycle at low ambient temperatures is not fully exploited. Unless the lowering of the chilled water temperature below the usual 7°C is beneficial for the air-conditioning system, a convenient way to exploit such potential would consist in controlling fan speed so to decrease the electricity consumption of the fan while keeping as high as possible cooling capacity and thermal COP.

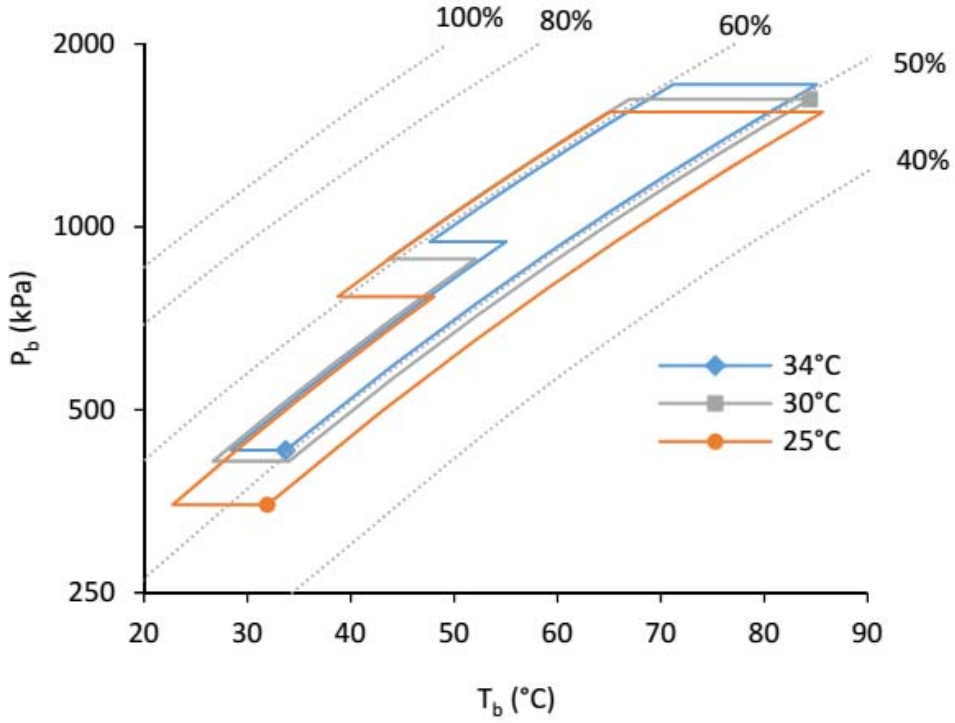

Fig. 9 – Solution cycle in the P-T-X diagram (model)

4.3 Effect of varying fan speed

The effect of varying fan speed, and the associated electricity consumption, around the reference point is investigated. As seen in Fig. 10, an increase of fan speed allows improving both cooling capacity and thermal COP at the expense of a higher electricity consumption, from 175 W up to 300 W. The combined effect is a reduction of electrical COP. The opposite trend is observed when fan speed is reduced and its consumption decreases from 175 W to 80 W. In this range, the gain in electrical COP tends to levels off, whereas a steep reduction of both capacity and thermal COP occurs. It is noticed that the electrical COP tends to attain its maximum at the minimum fan speed.

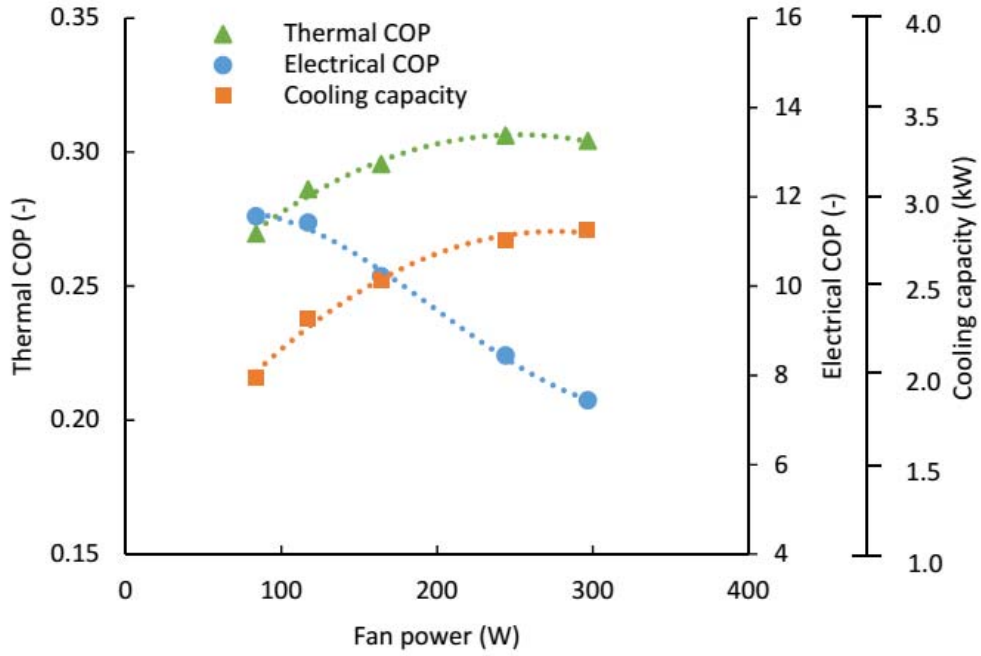

Fig. 10 – Effect of varying fan speed (experimental)

Temperature of weak solution does not change much with increasing fan speed, while condenser, absorber and evaporator pressures slightly diminish (see Fig. 11). As consequence of the decrease of condenser pressure, weak solution gets weaker, mass fractions spread out and more vapor is generated. The larger load at the absorber does not constitute a problem since a larger air flow improves heat exchange effectiveness. Therefore, also absorber pressure decreases, but slightly. In turn, also separator pressure decreases and so the refrigerant temperature in the RCA, which leads to lower pressure in the RCA solution and the evaporator.

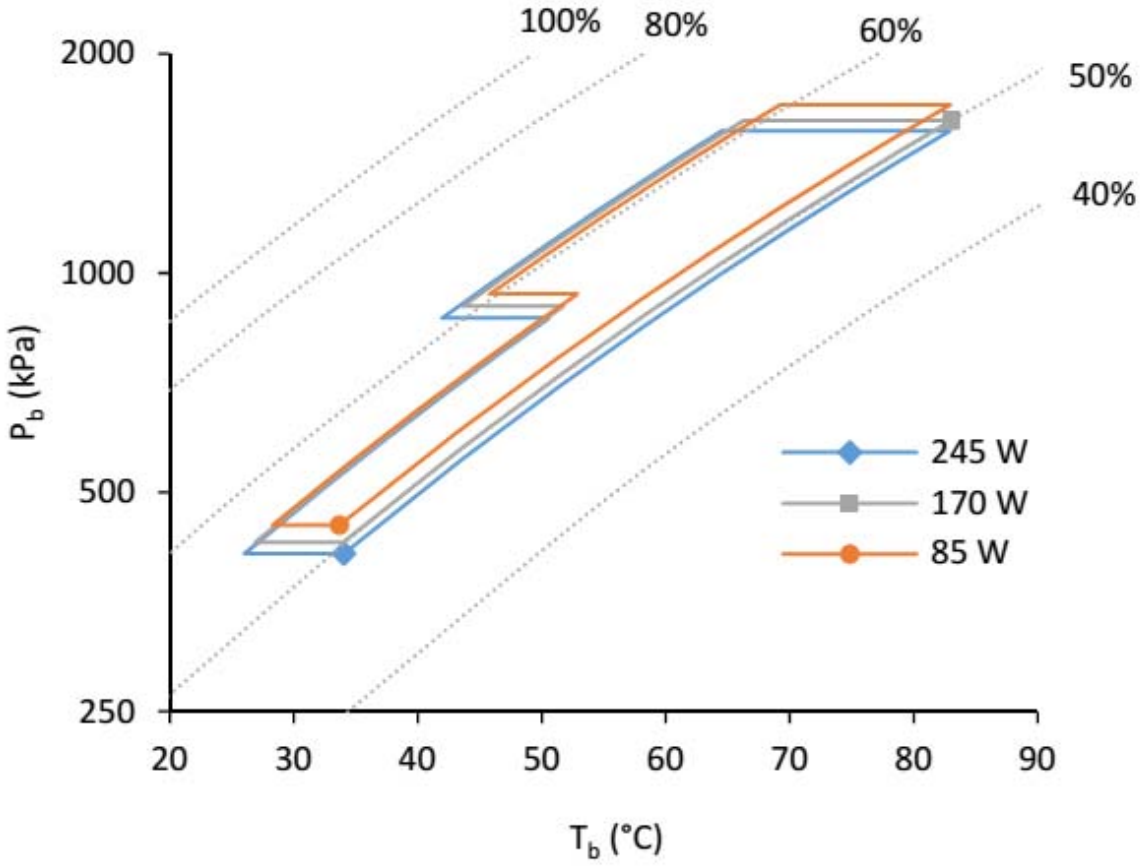

Fig. 11 – Effect of varying fan speed in the P-T-X diagram (model)

4.4 Effect of varying temperature drop and inlet temperature at the generator

The purpose of these tests is twofold. On the one hand, the effect of varying temperature drop and inlet temperature at the generator is investigated, as these are the usual ways to control cooling capacity. On the other hand, electrical COP is optimized by adopting a variable speed control strategy for the fan. The control strategy aims to increase fan speed for air temperatures above reference point (30 °C), so to contrast the drop in cooling capacity and thermal COP, and to decrease fan speed below reference point, in order to increase electrical COP. In practice, this is achieved by counteracting the pressure variation at the condenser due to varying air temperature.

As compared to reference conditions (90-80), the variable speed control strategy of the fan effectively reduces the sensitivity of cooling capacity to air temperature variations (see Fig. 12-a).

The average percentage decrease per air temperature degree is now 4.9% K^{-1} for cooling capacity. On the contrary, sensitivity of electrical COP decrease with air temperature increases to 15 % K^{-1} (see Fig. 12-c). Thermal COP varies between 0.26 and 0.31 and shows a regular trend within the air temperature range compatible with the temperatures at the generator (see Fig 12-b).

Moving hot water temperatures from 90-80 to 80-70, a large drop of cooling capacity is observed. For example, capacity at air temperature of 30°C drops from 2.5 kW to 1.6kW. The effect of reducing temperature drop, for constant inlet temperature of 80°C, is opposite. With air temperature of 30°C, capacity increases from 1.6 kW to 2.2 kW by lowering temperature drop from 10°C (80-70) to 5°C (80-75). It is interesting to notice the effect of varying the hot water temperature drop also in the P-T-X diagram (see Fig. 13). With a lower temperature drop (and so a higher flow rate), heat transfer rate between hot water stream and solution increases so that the concentrations spread out, more vapor is generated and capacity increases. Due to the higher load at the condenser and the two absorbers, the three pressures increase as well. Table 3 shows the effect on the main solution streams entering and leaving the generator, along with the variation of heat input and UA-value. It is noticed that the overall heat transfer coefficient increases by 32%. This suggests that reducing the cross section of the water stream in the generator, the heat transfer coefficient between water and tubes could be improved at low water flow rates, achieving larger heat inputs and cooling capacities. Although at parity of water flow rate pressure drops would be larger in the generator, a low-flow strategy can be preferable to a high-flow strategy in terms of overall parasitic consumption associated to the driving loop.

Table 3 – Effect of varying temperature drop at the generator (model)

T_{hwi} (°C)	T_{hwo} (°C)	$T_{GEN,i}$ (°C)	$T_{GEN,o}$ (°C)	Q_{GEN} (kW)	UA_{GEN} (kW/K)	$\dot{m}_{GEN,i}$ (kg/h)	$\dot{m}_{GEN,o}$ (kg/h)	$\dot{m}_{CON}$ (kg/h)	$X_{GEN,i}$ (kg/kg)	$X_{GEN,o}$ (kg/kg)
80	70	62.5	74.1	5.799	0.825	78.2	65.0	13.2	60.3%	52.2%
80	75	62.8	77.3	7.241	1.087	83.6	66.1	17.4	61.6%	51.5%

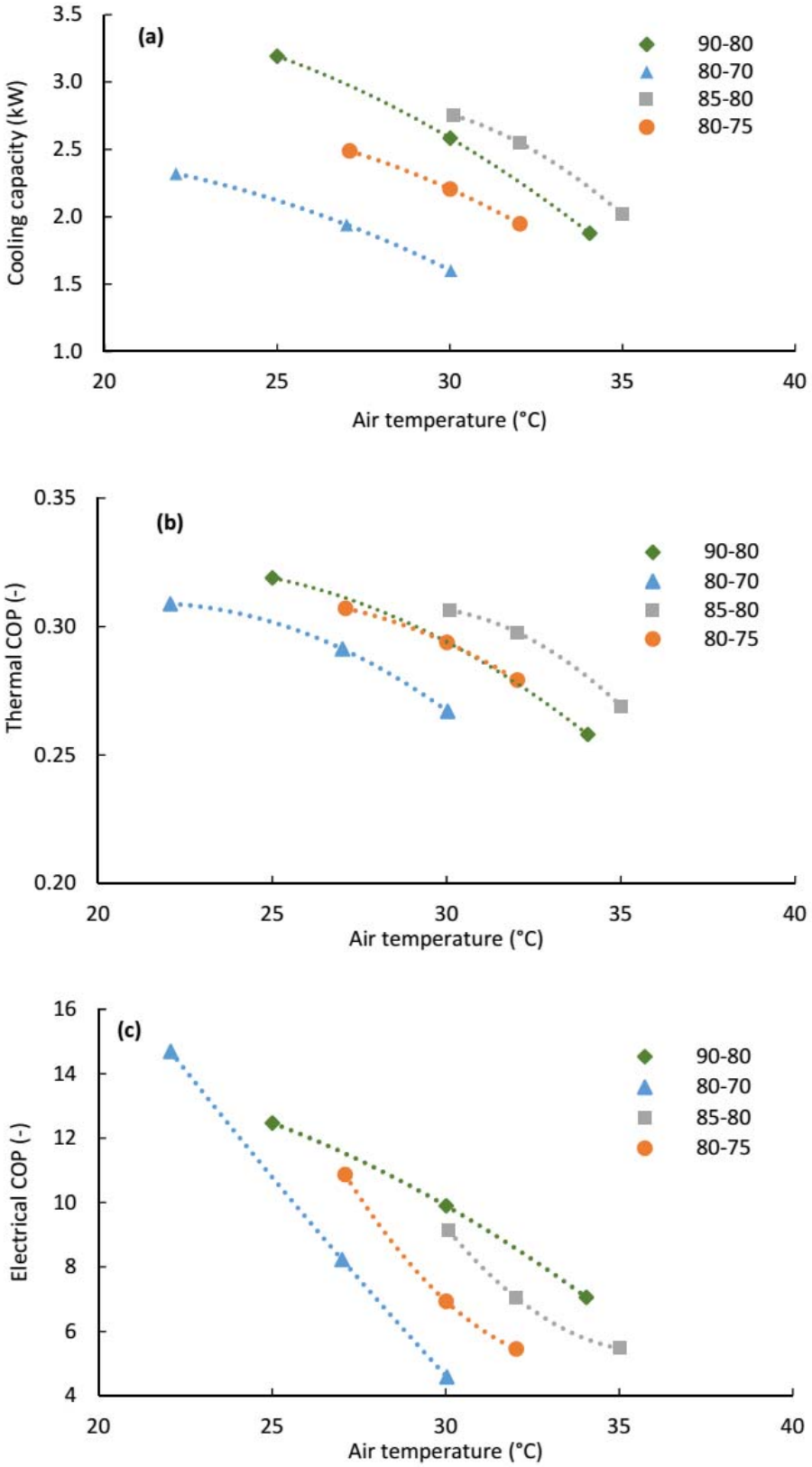

Fig. 12 – Effect of varying hot water temperatures on (a) cooling capacity, (b) thermal COP and (c) electrical COP (experimental)

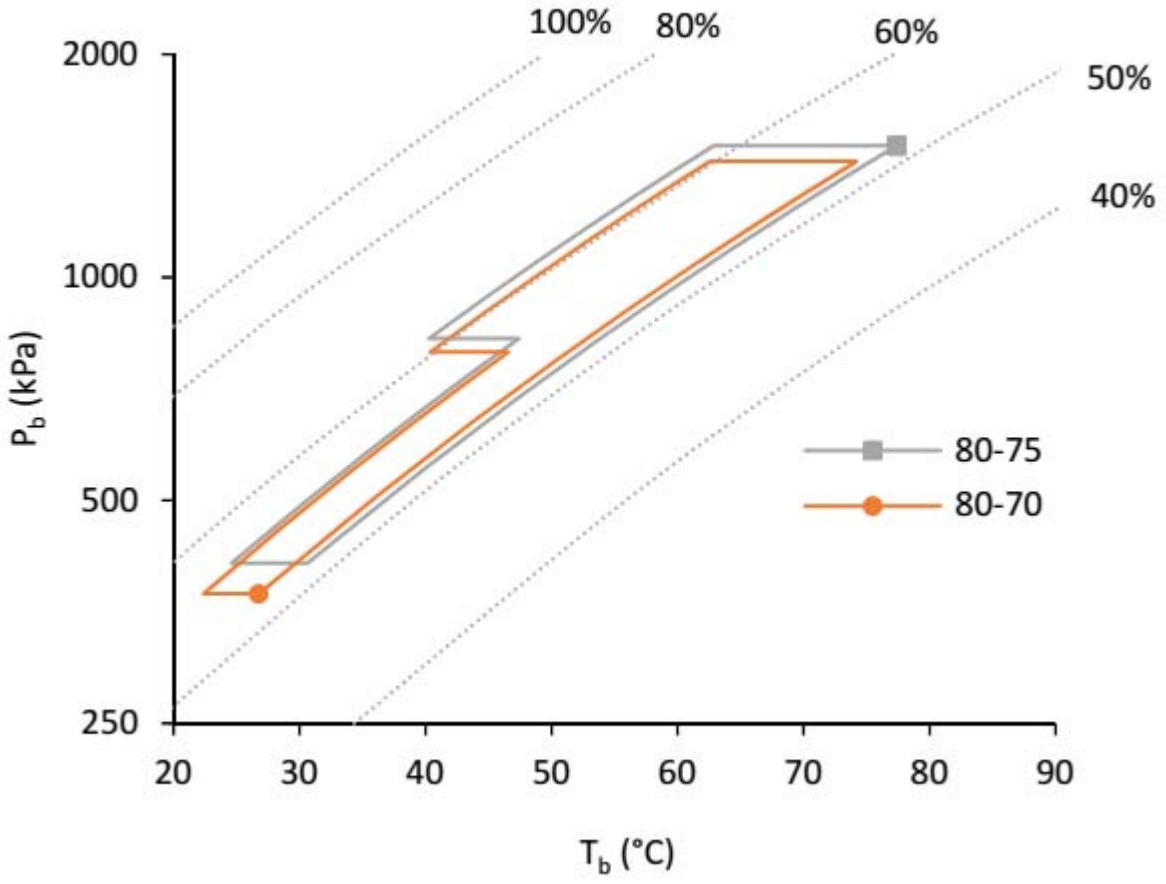

Fig. 13 – Effect of varying hot water temperature drop in the P-T-X diagram (model)

5. Conclusion

A prototype air-cooled double-lift NH3-H2O absorption refrigeration ystem has been experimentally investigated under different operating conditions that are of interest for air-conditioning applications. The unit operated steadily with chilled water temperature inlet 12°C, outlet 7°C, air temperature between 22°C and 38°C, and hot water driving temperatures variable from 80 to 90°C. The reference cooling capacity at air temperature 30°C is 2.5 kW, with thermal COP about 0.3 and electrical COP of 10. The unit turned out to perform smoothly, being able to adjust quickly to variable boundary conditions.

Moreover, through the mathematical modelling of the cycle and the experimental acquisition of heat input, cooling capacity and internal temperatures and pressures, a procedure for the identification of the unknown solution mass fractions and mass flow rates has been carried out. The identification has been achieved under certain hypotheses concerning the operation of the volumetric pumps and the relationship between pressure drop and mass flow rate in the weak solution line.

In the investigated chilled design, the splitting of the refrigerant mass flows between intermediate pressure and low pressure is self-adjusting thanks to the strong mutual influence existing between evaporator and refrigerant cooled absorber. However, a highly effective refrigerant cooled absorber is needed in order to keep a low enough pressure in the evaporator.

With the current design, the unit is best suited for applications in which the driving heat is delivered with a low temperature difference at the generator (e.g. 5°C), such as the direct coupling with internal combustion engines. As shown by the combined experimental and numerical data, the heat transfer at generator can be further optimized for applications like solar cooling, in which a low flow strategy for the driving circuit is permitted and can be beneficial for the overall system electrical COP. Thanks to the detailed data that can be obtained by the combined experimental and numerical analysis, future works can focus on the modelling and validation of the involved heat exchangers.

REFERENCES

Alefeld, G., Radermacher R., 1993. Heat conversion systems, CRC press.

Du, S., Wang, R. Z., Lin, P., Xu, Z. Z., Pan, Q.W., Xu, S.C., 2012. Experimental studies on an air-cooled two-stage NH3-H2O solar absorption air-conditioning prototype. Energy 45, 581-587.

Erickson, D.C., Tang J., 1996. Evaluation of double-lift cycles for waste heat powered refrigeration. ISHPC, Montreal, Canada, 161-168.

Grossman, G., Zaltash, A., 2001. ABSIM — modular simulation of advanced absorption systems. Int. J. Refrigeration 24, 531-543.

Guerra, M., 2012a. Self-adapting multi-stage absorption heat pump. Patent Publication No. EP2466229 A1.

Guerra, M., 2012b. Self adaptive refrigerant flow low temperature driven dual lift absorption cycle. 10th IIR Gustav Lorentzen Conference on Natural Refrigerants, Delft, The Netherlands, Paper No. 194.

Henning, H-M., Motta, M., Mugnier, D., 2013. Solar Cooling Handbook – A guide to solar assisted cooling and dehumidification, third ed. SpringerWien, New York.

Herold, K.E., Radermacher, R., Klein, S.A., 1996. Absorption Chillers and Heat Pumps, CRC Press.

Incropera, F.P., Dewitt, D.P., Bergman, T.L., Lavine, A.S., 2007. Fundamentals of Heat and Mass Transfer, sixth ed. John Wiley & Sons.

Kim, D.S., Infante Ferreira, C.A., 2005. Air Cooled Solar Absorption Air Conditioning Final Report. Delft University of technology, Delft, The Netherlands.

Kojasoy, G., Landis, F., Kwame-Mensah, P., Chang, C.T., 1997. Two-phase pressure drop in multiple thick- and thin-orifice plates. Experimental Thermal and Fluid Science 15, 347-358.

Wang, K., Abdelaziz, O., Kisari, P., Vineyard, E., 2011. State-of-the-art review on crystallization control technologies for water/LiBr absorption heat pumps. Int. J. Refrigeration 34, 1325-1337.

Ziegler, B., Trepp, C., 1984. Equation of state for ammonia-water mixtures, Int. J. Refrigeration 7, 101-106.

Ziegler, F., Alefeld, G., 1987. Coefficient of performance of multistage absorption cycles. Int. J. Refrigeration 10, 285–295.

Nomenclature

a_{P}	accuracy for pressures, Pa
a_{Q}	accuracy for heat transfer rates, W
a_{T}	accuracy for temperatures, K
C	heat capacity rate, W K^{-1}
C_r	heat capacity ratio, -
ΔT_{lm}	log mean temperature difference, K
h	enthalpy, J kg^{-1}
$\dot{m}$	mass flow rate, kg s^{-1}
P	pressure, Pa
Q	heat transfer rate, W
T	temperature, K
UA	overall heat transfer coefficient, W K^{-1}
$\dot{V}$	volume flow rate, m^3 s^{-1}
W	mechanical power, W
w_{P}	normalization weight for pressures, Pa^{-2}
w_{Q}	normalization weight for heat transfer rates, W^{-2}
w_{T}	normalization weight for temperatures, K^{-2}
X	ammonia mass fraction, kg kg^{-1}
x	vapor quality, kg kg^{-1}
$\boldsymbol{z}$	vector of model parameters

Greek symbols

ε	heat exchanger effectiveness, -
η	pump efficiency, -
ρ	density, kg m^{-3}

Subscripts

b	bubble point
e	electrical
G	gas phase at equilibrium
i	inlet
L	liquid phase at equilibrium
o	outlet
R	single effect refrigeration cycle
T	single effect heat transformer cycle
t	thermal

Abbreviations

ABS	absorber
aux	auxiliaries (fan, pumps)
CON	condenser
COP	coefficient of performance
cwi	chilled water inlet
cwo	chilled water outlet
EVA	evaporator
GEN	generator
hwi	hot water inlet
hwo	hot water outlet
NTU	number of transfer unit, -
RCA	refrigerant cooled absorber
REC	rectifier

RHE refrigerant heat exchanger

RMSE root mean square error, -

RS restrictor

SEP separator

SHE solution heat exchanger